Letters

Data-Driven Deadbeat Predictive Harmonic Current Control for Dual Three-Phase PMSM With Dynamic Linearization

Wusen Wang, *Member, IEEE*, Yuxin Chang, Ying Fan, *Senior Member, IEEE*, and Wei Hua, *Senior Member, IEEE*

***Abstract*—Harmonic currents inherently exist in a dual three-phase permanent magnet synchronous motor (DTP-PMSM) due to various disturbances, such as inverter nonlinearity and motor asymmetry. This letter proposes a data-driven deadbeat predictive harmonic current control (DD-DPHCC) method aimed at suppressing harmonic currents. First, a data-driven model of the harmonic currents for a DTP-PMSM is developed using dynamic linearization theory. This model exclusively relies on system input and output data to facilitate real-time updates, thereby eliminating the necessity for motor parameters. Then, a deadbeat control algorithm is designed to directly calculate the harmonic control voltage based on the sampled harmonic currents and the data-driven model, ensuring precise harmonic current control performance. Compared to conventional model-based DPHCC methods, the proposed DD-DPHCC exhibits enhanced robustness against motor parameter mismatches. Finally, experimental results substantiate the superior performance of the proposed DD-DPHCC method in suppressing harmonic currents.**

***Index Terms*—Deadbeat control, dual three-phase, dynamic linearization, harmonic currents, permanent magnet synchronous motor (PMSM).**

I. Introduction

DUAL three-phase permanent-magnet synchronous motors (DTP-PMSMs) attract much attention in high-performance applications due to their high power density and inherent fault tolerance. However, inverter-based PWM excitation in DTP-PMSMs inevitably generates harmonic currents, which arise not only from the switching process but also from nonideal effects such as dead-time and motor asymmetries. These harmonics result in torque ripple, acoustic noise, and efficiency deterioration, thus necessitating effective suppression strategies to ensure better performance.

Received 4 September 2025; revised 28 October 2025; accepted 6 November 2025. Date of publication 10 November 2025; date of current version 19 January 2026. This work was supported by the National Natural Science Foundation of China under Grant 52407039 and Grant 62173086. *(Corresponding author: Wusen Wang.)*

The authors are with the School of Electrical Engineering, Southeast University, Nanjing 210096, China (e-mail: wswang@seu.edu.cn; yxchang@seu.edu.cn; vickifan@seu.edu.cn; huawei1978@seu.edu.cn).

Color versions of one or more figures in this article are available at https://doi.org/10.1109/TPEL.2025.3631316.

Digital Object Identifier 10.1109/TPEL.2025.3631316

To mitigate harmonic currents in DTP-PMSM drives, three main categories of approaches have been extensively investigated. The first category focuses on the optimization of PWM strategies. Early 12-sector SVPWM controlled only the $\alpha\beta$ subspace, leading to significant low-order harmonics [1]. To address this, 24-sector SVPWM and its variants [2] were proposed to suppress xy subspace harmonics, albeit at the cost of reduced voltage utilization. Other variants, such as the five-active-vector SVPWM [3], provide improvements under certain conditions, but suffer from increased complexity and limited applicability.

The second category is improved linear current controllers. Proportional–resonant (PR) controllers [4] and multisynchronous-frame proportional-integral (PI) controllers [5] are widely adopted to selectively suppress harmonic components. Nevertheless, PR controllers are highly sensitive to frequency mismatch and may suffer from interharmonic interference, whereas multiframe PI controllers require low-pass filters to extract harmonic signals, which inevitably introduce estimation errors.

The third category explores model-based predictive control methods. Model predictive control minimizes a cost function to directly select appropriate voltage vectors and has demonstrated effective harmonic suppression [6]. However, the computational burden grows rapidly with the number of candidate vectors increasing, which limits its real-time feasibility. Deadbeat predictive harmonic current control (DPHCC) provides deadbeat performance in harmonic current suppression. However, it strongly depends on the accuracy of system models, and its robustness is severely degraded under parameter mismatches. To enhance robustness, disturbance observers such as extended state observers have been integrated with predictive control to compensate for modeling uncertainties [7], [8].

Different from conventional model-based controllers, data-driven control (DDC) avoids explicit reliance on accurate motor models, thereby mitigating the negative impact of parameter mismatches. Among DDC methods, model-free adaptive control [9] is a typical approach that employs dynamic linearization theory to construct an equivalent model in real time, where system dynamics are characterized by pseudopartial derivatives (PPDs) updated iteratively.

This letter proposes a novel control strategy that integrates DDC with deadbeat control to suppress harmonic currents in

DTP-PMSM drives. First, a data-driven model of the DTP-PMSM is established using the dynamic linearization framework. Then, an iterative formulation to update the PPD matrix is developed to enable accurate online model adaptation. Finally, based on the data-driven model, current prediction, and voltage generation are carried out with a deadbeat pattern. Experimental results demonstrate the effectiveness and advantages of the proposed method in harmonic suppression.

II. Motor Model and Conventional DPHCC

A. Mathematical Model of DTP-PMSM

In multiphase motor drive systems, the vector space decoupling (VSD) [10] method is usually employed to map the variables of each motor phase to different harmonic subspaces. The VSD transformation of the DTP-PMSM is as follows:

$$[f_\alpha\ f_\beta\ f_x\ f_y\ f_{o_1}\ f_{o_2}]^T = \mathbf{T}_{\text{VSD}} \cdot [f_{A1}\ f_{B1}\ f_{C1}\ f_{A2}\ f_{B2}\ f_{C2}]^T \tag{1}$$

where f is the motor stator variables, such as voltage u, current i, and flux ψ. The VSD transformation matrix is

$$\mathbf{T}_{\text{VSD}} = \frac{1}{3}\begin{bmatrix} 1 & -1/2 & -1/2 & \sqrt{3}/2 & -\sqrt{3}/2 & 0 \\ 0 & \sqrt{3}/2 & -\sqrt{3}/2 & 1/2 & 1/2 & -1 \\ 1 & -1/2 & -1/2 & -\sqrt{3}/2 & \sqrt{3}/2 & 0 \\ 0 & -\sqrt{3}/2 & \sqrt{3}/2 & 1/2 & 1/2 & -1 \\ 1 & 1 & 1 & 0 & 0 & 0 \\ 0 & 0 & 0 & 1 & 1 & 1 \end{bmatrix}. \tag{2}$$

With the transformation, the variables of the DTP-PMSM are mapped onto three orthogonal harmonic subspaces: $\alpha\beta$ subspace, xy subspace, and o_1o_2 subspace. The fundamental components are projected onto the $\alpha\beta$ subspace, where they produce a rotating magnetic motive force and contribute to electromechanical energy conversion. The fifth- and seventh-order components are mapped to the xy subspace. Besides, the third-order components are mapped to the o_1o_2 subspace, also known as the zero-sequence subspace, which can be neglected due to the star-connection windings.

Since the components in the xy subspace dominate the harmonics in DTP-PMSM, only the xy subspace model is considered in this manuscript. In the xy subspace, the mathematical model of DTP-PMSM can be derived as

$$\mathbf{u}_{xy} = \begin{bmatrix} R_s + L_{xy}s & 0 \\ 0 & R_s + L_{xy}s \end{bmatrix} \mathbf{i}_{xy} + \mathbf{E}_{xy} \tag{3}$$

where $\mathbf{u}_{xy}$ and $\mathbf{i}_{xy}$ are the stator voltage and current in the xy subspace. $\mathbf{u}_{xy} = [u_x, u_y]^T$, $\mathbf{i}_{xy} = [i_x, i_y]^T$. L_{xy} is the stator leakage inductance. R_s is the stator resistance. s represents a derivative operator. $\mathbf{E}_{xy}$ is the back-EMF harmonics term related to the rotor position θ. $\mathbf{E}_{xy} = [E_x, E_y]^T$.

Furthermore, to implement the motor control algorithms in a real-time digital microcontroller, it is necessary to convert the mathematical model of DTP-PMSM into a discrete form. According to (3), the xy subspace mathematical model can be discretized based on zero-order hold as

$$\mathbf{i}_{xy}\ (k+1) = A\mathbf{i}_{xy}(k) + B\mathbf{u}_{xy}(k) - \frac{A}{L_{xy}}\int_{kT_s}^{(k+1)T_s} e^{-\frac{R_s}{L_{xy}}t} \cdot \mathbf{E}_{xy}(t)\, dt \tag{4}$$

where $A = e^{-\frac{R_s T_s}{L_{xy}}}$, $B = (1-A)/R_s$.

B. Conventional DPHCC

When designing a deadbeat control, it is essential to account for the one control period delay resulting from the intrinsic property of PWM updating in digital controllers. Therefore, in the (k)th control period, DPHCC strategy first predicts the currents in the $(k+1)$th control period as

$$\mathbf{i}_{xy}^{\text{pre}}\ (k+1) = A\mathbf{i}_{xy}(k) + B\mathbf{u}_{xy}(k) - \mathbf{D}_{xy}(k) \tag{5}$$

where $\mathbf{D}_{xy}$ is the lumped disturbance term related to back-EMF harmonics $\mathbf{E}_{xy}$ and other unmodeled errors.

Then, the control voltage reference in the $(k+1)$th control period $\mathbf{u}_{xy}^{ref}(k+1)$ can be calculated with the current reference in the $(k+2)$th control period $\mathbf{i}_{xy}^{ref}(k+2)$ as

$$\mathbf{u}_{xy}^{ref}\ (k+1) = \frac{1}{B}\mathbf{i}_{xy}^{ref}(k+2) - \frac{A}{B}\mathbf{i}_{xy}^{\text{pre}}(k+1) + \frac{1}{B}\mathbf{D}_{xy}(k+1). \tag{6}$$

Additionally, a disturbance observer needs to be designed to estimate the lumped disturbance $\mathbf{D}_{xy}$.

According to (5) and (6), a major drawback of the conventional DPHCC is its heavy dependence on motor parameter accuracy. However, these parameters vary and are difficult to measure precisely in the xy subspace.

III. Data-Driven Harmonic Current Suppression

To overcome the limitation of conventional DPHCC, a data-driven deadbeat predictive harmonic current control (DD-DPHCC) method is designed in this section, which is independent of motor parameters.

A. Data-Driven Model of DTP-PMSM

Due to the inaccuracy and variation of motor parameters as well as other unmodeled disturbances, the coefficients A and B in (4) are nonlinear variables. Thus, (4) can be reformulated as a multi-input multioutput (MIMO) nonlinear system as

$$\mathbf{i}_{xy}\ (k+1) = f(\mathbf{i}_{xy}(k), \mathbf{u}_{xy}(k)). \tag{7}$$

Since (7) corresponds to a physical DTP-PMSM, it should satisfy the *Lipschitz* continuity condition during each control period, thereby bounding the sensitivity of the output to input perturbations and ensuring model stability. This can be expressed as

$$\|\Delta\mathbf{i}_{xy}(k+1)\| \le b\|\Delta\mathbf{H}(k)\| \tag{8}$$

where b is a positive constant, $\Delta\mathbf{H}(k) = \mathbf{H}(k) - \mathbf{H}(k-1)$, $\mathbf{H}(k)$ is a composite matrix including input and output vectors

$$\mathbf{H}\ (k) = \left[\mathbf{i}_{xy}(k)^T, \mathbf{u}_{xy}(k)^T\right]^T. \tag{9}$$

To develop a control system for the MIMO nonlinear system (7), dynamic linearization theory is utilized.

According to the discrete-time model (4), an incremental form of the model can be further derived by subtracting the discrete-time model at two adjacent sampling instants as

$$\Delta \mathbf{i}_{xy}\ (k+1) = A\Delta \mathbf{i}_{xy}\,(k) + B\Delta \mathbf{u}_{xy}\,(k) - \Delta \mathbf{E}^{*}_{xy}\,(k) \tag{10}$$

in which

$$\Delta \mathbf{i}_{xy}\ (k) = \mathbf{i}_{xy}\ (k) - \mathbf{i}_{xy}\,(k-1) \tag{11}$$

$$\Delta \mathbf{u}_{xy}\ (k) = \mathbf{u}_{xy}\ (k) - \mathbf{u}_{xy}\,(k-1) \tag{12}$$

$$\Delta \mathbf{E}^{*}_{xy}\ (k) = \mathbf{E}^{*}_{xy}\ (k) - \mathbf{E}^{*}_{xy}\,(k-1)\,. \tag{13}$$

$\mathbf{E}^{*}_{xy}(k)$ represents the whole last term in (4).

Then, the incremental model (10) can be reformulated into a full form dynamic linearization (FFDL) model as

$$\Delta \mathbf{i}_{xy}\ (k+1) = \mathbf{\Phi}_{f}\ (k)\,\Delta \mathbf{H}\,(k)\,. \tag{14}$$

Compared with (10), $\Delta \mathbf{i}_{xy}(k)$ and $\Delta \mathbf{u}_{xy}(k)$ are included in $\Delta \mathbf{H}(k)$. $\Delta \mathbf{E}^{*}_{xy}(k)$ is regarded as a disturbance term and is eliminated since its values cannot be measured.

The PPD matrix $\mathbf{\Phi}_f$ in (14) is updated in each control period based on the input and output data of the system. Therefore, it can effectively capture the input–output relationship as well as absorb the influence of those unmodeled nonlinearities and disturbances, such as $\Delta \mathbf{E}^{*}_{xy}$. According to (9), (11), and (12), $\Delta \mathbf{H}(k)$ contains both the current term and the voltage term and is a vector with 4×1 dimensions. Thus, the PPD matrix should be of 2×4 dimensions and can be expressed as

$$\mathbf{\Phi}_{f} = \begin{bmatrix} \mathbf{\Phi}_{fi} & \mathbf{\Phi}_{fu} \end{bmatrix} \tag{15}$$

$$\mathbf{\Phi}_{fi} = \begin{bmatrix} \phi_{i11} & \phi_{i12} \\ \phi_{i21} & \phi_{i22} \end{bmatrix} \tag{16}$$

$$\mathbf{\Phi}_{fu} = \begin{bmatrix} \phi_{u11} & \phi_{u12} \\ \phi_{u21} & \phi_{u22} \end{bmatrix}\,. \tag{17}$$

To ensure model stability and boundedness, the norm of the PPD matrix should satisfy the following condition:

$$\|\mathbf{\Phi}_{f}\| \le b. \tag{18}$$

Subsequently, the FFDL modeling process of DTP-PMSM becomes determining $\mathbf{\Phi}_f$. If the estimated $\mathbf{\Phi}_f$ in the $(k-1)$th control period is $\hat{\mathbf{\Phi}}_f(k-1)$, $\Delta \mathbf{i}_{xy}(k)$ can then be predicted according to (14) as

$$\Delta \mathbf{i}^{\text{pre}}_{xy}\ (k) = \hat{\mathbf{\Phi}}_{f}\ (k-1)\,\Delta \mathbf{H}\,(k-1)\,. \tag{19}$$

Then, in (k)th control period, an error function can be developed to judge the prediction error as

$$J\ (\mathbf{\Phi}_{f}) = \|\Delta \mathbf{i}_{xy}\,(k) - \Delta \mathbf{i}^{pre}_{xy}\,(k)\,\|^{2}. \tag{20}$$

The gradient of the error function with respect to the PPD matrix is calculated to obtain the steepest descent direction of the squared error, as (21), which subsequently serves as the iterative update direction for the PPD matrix

$$\frac{\partial J\left(\hat{\mathbf{\Phi}}_{f}\right)}{\partial \hat{\mathbf{\Phi}}_{f}}$$

$$= -2\left[\Delta \mathbf{i}_{xy}\,(k) - \hat{\mathbf{\Phi}}_{f}\,(k-1)\,\Delta \mathbf{H}\,(k-1)\right]\Delta \mathbf{H}(k-1)^{T}. \tag{21}$$

The PPD matrix can then be iteratively modified based on gradient descent theory as

$$\hat{\mathbf{\Phi}}_{f}\ (k) = \hat{\mathbf{\Phi}}_{f}\ (k-1) - \mu\frac{\partial J\left(\hat{\mathbf{\Phi}}_{f}\right)}{\partial \hat{\mathbf{\Phi}}_{f}} \tag{22}$$

where μ is a tuning parameter used to control the step size of the iteration. Then, by considering the power of $\mathbf{\Delta H}(k-1)$, the PPD matrix is updated as

$$\begin{aligned}\hat{\mathbf{\Phi}}_{f}\ (k) = \hat{\mathbf{\Phi}}_{f}\ (k-1) \\ + \frac{\mu}{\|\Delta \mathbf{H}\,(k-1)\,\|^{2}+\varepsilon} \\ \cdot \left[\Delta \mathbf{i}_{xy}\,(k) - \hat{\mathbf{\Phi}}_{f}\,(k-1)\,\Delta \mathbf{H}\,(k-1)\right]\Delta \mathbf{H}(k-1)^{T}\end{aligned} \tag{23}$$

where μ should satisfy $0<\mu<2$ for the stability of the gradient descent iteration. ε is a small positive constant introduced to avoid division by zero. Besides, in (23), $\|\Delta \mathbf{H}(k-1)\|^2$ equals to $\Delta i_x(k-1)^2 + \Delta i_y(k-1)^2 + \Delta u_x(k-1)^2 + \Delta u_y(k-1)^2$ so that the second line of (23) is scalar. In the last line, the first term is the error of $\Delta \mathbf{i}_{xy}(k)$, which is a vector with 2×1 dimensions. Since $\Delta \boldsymbol{H}(k-1)^T$ is a vector with 1×4 dimensions, the last line of (23) is a matrix with 2×4 dimensions, which is the same as the PPD matrix $\mathbf{\Phi}_f$. As a result, the gradient descent updating of the PPD matrix $\mathbf{\Phi}_f$ with (23) is vectorized.

Ultimately, (14) represents the data-driven model of the DTP-PMSM in the xy subspace, with equation (23) used for updating the PPD matrix.

B. Parameter Design for PPD Matrix Iteration

In the PPD matrix iteration process, the parameters involve the initial values of the PPD matrix $\mathbf{\Phi}_f$, μ, and ε.

Based on (9) to (14), the values of the elements in $\mathbf{\Phi}_f$ are related to A and B in (4). Hence, the PPD matrix $\mathbf{\Phi}_f$ can be initialized with A and B as

$$\mathbf{\Phi}_{f}\ (0) = \begin{bmatrix} A & 0 & B & 0 \\ 0 & A & 0 & B \end{bmatrix}. \tag{24}$$

According to (23), ε is a small positive constant, which can be set as 1e-6. μ is between $(0,\ 2)$ and is the only parameter that needs to be tuned.

Define the last line of (23) as

$$\mathbf{C}_{\mathbf{\Phi}} = \left[\Delta \mathbf{i}_{xy}\,(k) - \hat{\mathbf{\Phi}}_{f}\,(k-1)\,\Delta \mathbf{H}\,(k-1)\right]\ \Delta \mathbf{H}(k-1)^{T}. \tag{25}$$

TABLE I
PARAMETERS OF THE TESTED DTP-PMSM

Symbol	Parameter	Value
p_n	Pole pairs	5
R_s	Stator resistance	2 Ω
L_d	d-axis inductance	5 mH
L_q	q-axis inductance	8 mH
L_{xy}	Stator leakage inductance	2 mH
ψ_{pm}	Flux linkage of PM	0.07 Wb
J	Rotational inertia	0.0006 kg·m^2
n_N	Rated speed	1000 r/min
T_N	Rated torque	2 N·m

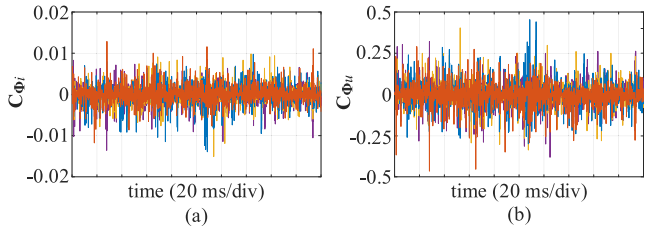

Fig. 1. Simulation results of $\mathbf{C}_{\mathbf{\Phi}}$. (a) Results of $\mathbf{C}_{\mathbf{\Phi}i}$. (b) Results of $\mathbf{C}_{\mathbf{\Phi}u}$.

$\mathbf{C}_{\mathbf{\Phi}}$ is a 2×4 matrix and can be rewritten as

$$\mathbf{C}_{\mathbf{\Phi}} = \begin{bmatrix} \mathbf{C}_{\mathbf{\Phi}i} & \mathbf{C}_{\mathbf{\Phi}u} \end{bmatrix} \tag{26}$$

$$\mathbf{C}_{\mathbf{\Phi}i} = \begin{bmatrix} \mathbf{C}_{\mathbf{\Phi}}(1,1) & \mathbf{C}_{\mathbf{\Phi}}(1,2) \\ \mathbf{C}_{\mathbf{\Phi}}(2,1) & \mathbf{C}_{\mathbf{\Phi}}(2,2) \end{bmatrix} \tag{27}$$

$$\mathbf{C}_{\mathbf{\Phi}u} = \begin{bmatrix} \mathbf{C}_{\mathbf{\Phi}}(1,3) & \mathbf{C}_{\mathbf{\Phi}}(1,4) \\ \mathbf{C}_{\mathbf{\Phi}}(2,3) & \mathbf{C}_{\mathbf{\Phi}}(2,3) \end{bmatrix}. \tag{28}$$

Refer to (15) to (17), $\mathbf{C}_{\mathbf{\Phi}i}$ is used to update $\mathbf{\Phi}_{fi}$, and $\mathbf{C}_{\mathbf{\Phi}u}$ is used to update $\mathbf{\Phi}_{fu}$.

Then, with the parameters of the tested DTP-PMSM, as listed in Table I, the simulation results of $\mathbf{C}_{\mathbf{\Phi}}$ are analyzed. The results are presented in Fig. 1. It can be observed that the values of $\mathbf{C}_{\mathbf{\Phi}i}$ are relatively small, while those of $\mathbf{C}_{\mathbf{\Phi}u}$ are much larger. However, according to the motor parameters, A is about 0.9, and B is about 0.05 in (24). The elements in $\mathbf{\Phi}_{fi}$ would be much larger than those in $\mathbf{\Phi}_{fu}$. Therefore, the μ used for $\mathbf{\Phi}_{fi}$ updating, defined as μ_i, can be much larger than the μ used for $\mathbf{\Phi}_{fu}$ updating, defined as μ_u. Comparing the values of $\mathbf{\Phi}_{fi}$, $\mathbf{\Phi}_{fu}$, $\mathbf{C}_{\mathbf{\Phi}i}$, and $\mathbf{C}_{\mathbf{\Phi}u}$, μ_i can be set around 1, and μ_u can be set around 0.01.

In addition, to prevent the PPD matrix from changing rapidly due to unexpected errors or undesired values of $\|\Delta\mathbf{H}(k-1)\|^2$, a limitation is set for the element change of the PPD matrix. If one of the elements in $|\hat{\mathbf{\Phi}}_{fi}(k) - \hat{\mathbf{\Phi}}_{fi}(k-1)|$ is larger than 0.1 or one of the elements in $|\hat{\mathbf{\Phi}}_{fu}(k) - \hat{\mathbf{\Phi}}_{fu}(k-1)|$ is larger than 0.01, $\hat{\mathbf{\Phi}}_f\ (k) = \hat{\mathbf{\Phi}}_f\ (k-1)$.

C. Proposed DD-DPHCC

Similar to the conventional DPHCC, when designing the proposed DD-DPHCC method, the one control period delay should also be considered. During the (k)th control period, the xy subspace currents in the $(k+1)$th control period should be predicted, and then calculate the control voltage reference for the $(k+1)$th control period accordingly.

According to (14), the xy subspace currents in the $(k+1)$th control period are predicted as

$$\mathbf{i}_{xy}^{\text{pre}}\ (k+1) = \mathbf{i}_{xy}\ (k) + \hat{\mathbf{\Phi}}_f\,(k)\,\Delta\mathbf{H}\,(k)\,. \tag{29}$$

Then, based on the deadbeat control theory, during the $(k+1)$th control period, the xy subspace currents should be controlled to their reference values $\mathbf{i}_{xy}^{ref}(k+2)$ with the control voltage reference $\mathbf{u}_{xy}^{ref}(k+1)$ as

$$\Delta\mathbf{i}_{xy}^{ref}\ (k+2) = \hat{\mathbf{\Phi}}_f\ (k+1)\,\Delta\mathbf{H}_{\text{pre}}\,(k+1) \tag{30}$$

where

$$\Delta\mathbf{i}_{xy}^{ref}\ (k+2) = \mathbf{i}_{xy}^{ref}\ (k+2) - \mathbf{i}_{xy}^{\text{pre}}\,(k+1) \tag{31}$$

$$\Delta\mathbf{H}_{\text{pre}}\ (k+1) = \left[\Delta\mathbf{i}_{xy}^{\text{pre}}(k+1)^T \quad \Delta\mathbf{u}_{xy}^{ref}(k+1)^T\right]^T \tag{32}$$

$$\Delta\mathbf{u}_{xy}^{ref}\ (k+1) = \mathbf{u}_{xy}^{ref}\ (k+1) - \mathbf{u}_{xy}\,(k)\,. \tag{33}$$

For the purpose of harmonic current suppression, $\mathbf{i}_{xy}^{ref}(k+2)$ can be set as 0.

In (30), the update of the PPD matrix $\hat{\mathbf{\Phi}}_f(k+1)$ follows the iteration rule (23), given by

$$\begin{aligned}\hat{\mathbf{\Phi}}_f\ (k+1) = \hat{\mathbf{\Phi}}_f\ (k) \\ + \frac{\mu}{\|\Delta\mathbf{H}\,(k)\,\|^2+\varepsilon} \\ \cdot\left[\Delta\mathbf{i}_{xy}^{\text{pre}}\,(k+1) - \hat{\mathbf{\Phi}}_f\,(k)\,\Delta\mathbf{H}\,(k)\right]\Delta\mathbf{H}(k)^T.\end{aligned} \tag{34}$$

According to (29), it is obvious that

$$\hat{\mathbf{\Phi}}_f\ (k+1) = \hat{\mathbf{\Phi}}_f\ (k)\,. \tag{35}$$

Eventually, the control voltage reference $\mathbf{u}_{xy}^{ref}(k+1)$ is calculated based on (30) as

$$\begin{aligned}\mathbf{u}_{xy}^{ref}\ (k+1) = \mathbf{u}_{xy}\ (k) \\ + \hat{\mathbf{\Phi}}_{fu}(k)^{-1}\left(\Delta\mathbf{i}_{xy}^{ref}\ (k+2) - \hat{\mathbf{\Phi}}_{fi}\,(k)\,\Delta\mathbf{i}_{xy}^{pre}\,(k+1)\right).\end{aligned} \tag{36}$$

The flowchart of the proposed DD-DPHCC algorithm is presented in Fig. 2. Compared with the conventional DPHCC, the proposed DD-DPHCC is developed totally based on the system input and output data, without using motor parameters. Thus, the proposed DD-DPHCC can be more robust and accurate than the conventional DPHCC. Besides, introducing a disturbance observer to DPHCC can improve robustness [7]. However, there are three coupled parameters in the observer that need to be tuned carefully. This makes the controller design process intricate. On the contrary, in the proposed DD-DPHCC, only the μ in (23) needs to be tuned. The design process becomes much more straightforward.

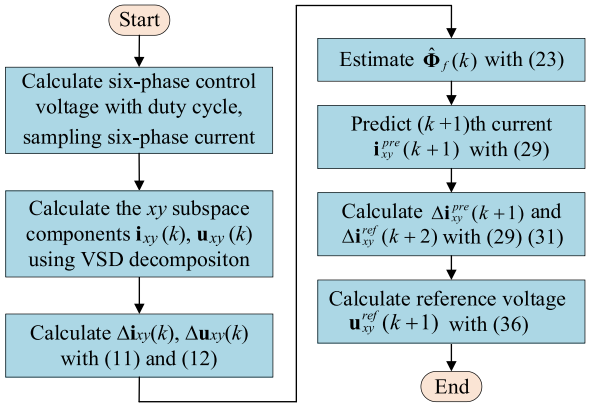

Fig. 2. Flowchart of the proposed DD-DPHCC algorithm.

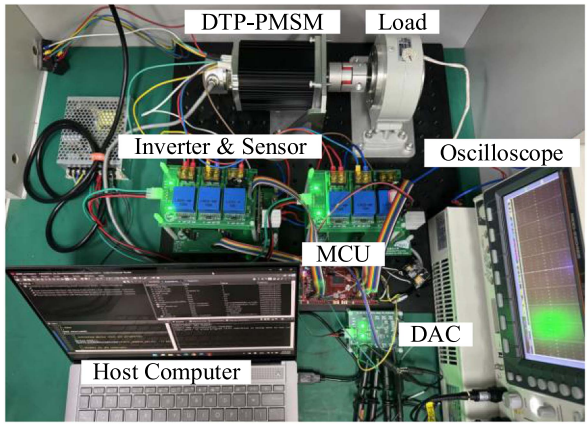

Fig. 3. Experimental platform of the tested DTP-PMSM.

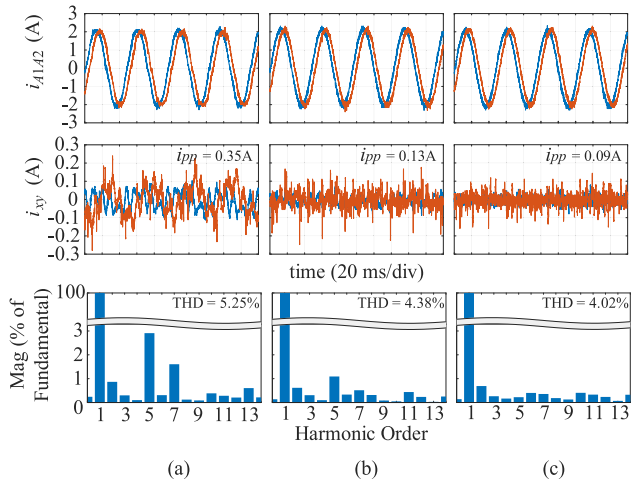

Fig. 4. Experimental results of the stator currents at 500 r/min and 2 N·m. (a) No harmonic current control. (b) DPHCC. (c) Proposed DD-DPHCC.

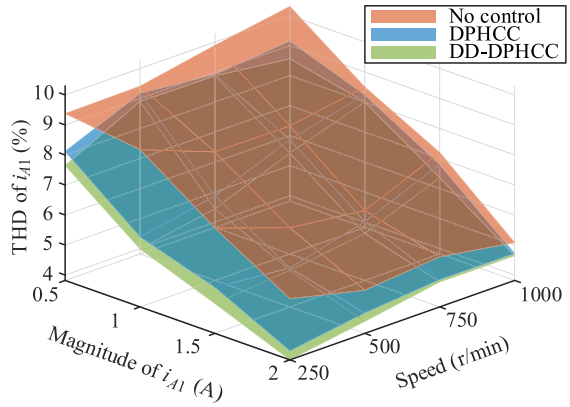

Fig. 5. Experimental results of the phase current THD under different rotor speed and load torque conditions.

IV. Experimental Validation and Analysis

To validate the harmonic suppression capability of the proposed DD-DPHCC method, comparative experiments have been conducted on a DTP-PMSM. The experiment platform is shown in Fig. 3. The parameters of the DTP-PMSM are listed in TABLE I in Section III. The digital controller is a TI microcontroller development kit, LAUNCHXL-F28379D. Both the sampling frequency and control frequency are 10 kHz. The sampling process is triggered by PWM at the beginning of every control period. The dead-time is 2 μs, and the dc bus voltage is 72 V.

A. Steady State Performance

The stator current results at 500 r/min and 2 N·m are shown in Fig. 4. Compared to the condition without harmonic current control, both DPHCC and the proposed DD-DPHCC can effectively suppress the harmonic currents in the xy subspace, especially the fifth and seventh order harmonics. In addition, the proposed DD-DPHCC performs better than DPHCC. Ignoring noise pulse signals, DD-DPHCC reduces the peak-to-peak value of the xy subspace current from 0.13 A with DPHCC to 0.09 A, and lowers the total harmonic distortion (THD) from 4.38% to 4.02% . This improvement is because L_{xy} used in DPHCC is not absolutely accurate. In contrast, the proposed DD-DPHCC uses a data-driven, real-time updated motor model, making it more accurate than DPHCC.

In Fig. 5 , the comparison of phase current THD across different rotor speeds and loads is presented to further verify the performance of the data-driven method. It illustrates that the proposed DD-DPHCC suppresses harmonic currents more effectively than DPHCC under all operating conditions.

B. Transient State Performance

Fig. 6 presents the experimental results with a 2 N·m load torque when the speed reference changes from 500 to 1000 r/min. Fig. 7 shows the experimental results at 500 r/min speed when the load torque changes from 0 to 2 N·m. These results illustrate that both conventional DPHCC and the proposed DD-DPHCC can suppress the harmonic currents effectively during the transient states. According to Figs. 6(b), 6(c), 7(b), and 7(c), the harmonic current suppression performance of the proposed DD-DPHCC is a bit better than the conventional DPHCC. This demonstrates the superiority of the proposed DD-DPHCC. Besides, since harmonic current suppression methods are implemented in the

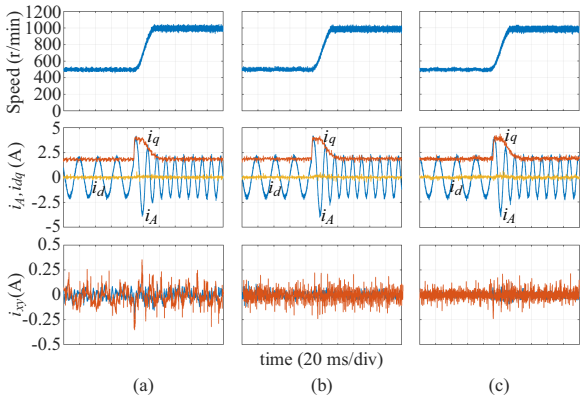

Fig. 6. Experimental results with 2 N·m load torque when the speed reference changes from 500 to 1000 r/min. (a) No harmonic current control. (b) DPHCC. (c) Proposed DD-DPHCC.

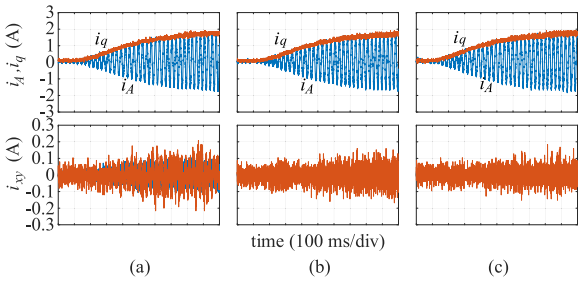

Fig. 7. Experimental results at 500 r/min speed when the load torque changes from 0 to 2 N·m. (a) No harmonic current control. (b) DPHCC. (c) Proposed DD-DPHCC.

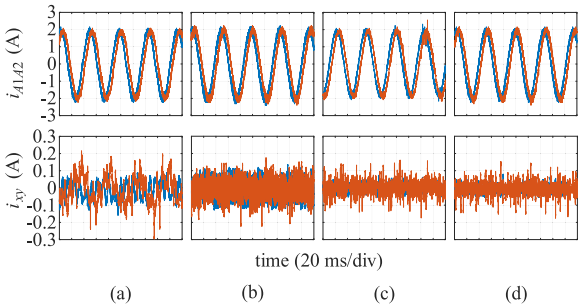

Fig. 8. Experimental results of the stator currents under three times L_{xy} error at 500 r/min and 2 N·m. (a) No harmonic current control. (b) DPHCC. (c) DPHCC with a disturbance observer. (d) Proposed DD-DPHCC.

xy subspace, similar responses in speed, phase currents, and dq-axis currents are observed across different control strategies.

C. Parameter Mismatch Performance

Fig. 8 shows the results under three times L_{xy} error at 500 r/min and 2 N·m. DPHCC suffers severe performance deterioration and even instability due to the parameter error, since it is derived from the motor model and its performance highly depends on the parameter accuracy. With a disturbance observer, as introduced in [7], the DPHCC method can work stably again. As shown in Fig. 8(c), the xy subspace harmonic currents are suppressed to about 0.14 A peak-to-peak if ignoring noise pulse signals. As for the proposed DD-DPHCC, it maintains stable operation and suppresses the xy subspace harmonic currents to about 0.1 A peak-to-peak.

V. Conclusion

This letter proposes a DD-DPHCC method to suppress harmonic currents in DTP-PMSMs. The DD-DPHCC scheme is designed based on a data-driven model of DTP-PMSM and operates in a deadbeat control pattern. Experimental results have been provided to validate the effectiveness of the proposed method. The following contributions have been achieved.

1) The proposed DD-DPHCC provides improved harmonic current suppression compared to the conventional DPHCC under all operating conditions.
2) The proposed DD-DPHCC is completely independent of motor parameters, ensuring consistent performance when motor parameters change.

References

[1] K. Gopakumar, V. T. Ranganthan, and S. R. Bhat, "Split-phase induction motor operation from PWM voltage source inverter," *IEEE Trans. Ind. Appl.*, vol. 29, no. 5, pp. 927–932, Sep./Oct. 1993.

[2] S. M. Suhel and R. Maurya, "Realization of 24-sector SVPWM with new switching pattern for six-phase induction motor drive," *IEEE Trans. Power Electron.*, vol. 34, no. 6, pp. 5079–5092, Jun. 2019.

[3] K. Cui, C. Wang, M. Zhou, and S. Sun, "Comprehensive investigation of space-vector PWM including novel switching sequences for dual three-phase motor drives," *IEEE Trans. Transport. Electrific.*, vol. 9, no. 1, pp. 1350–1362, Mar. 2023.

[4] M. Hu, W. Hua, G. Ma, S. Xu, and W. Zeng, "Improved current dynamics of proportional-integral-resonant controller for a dual three-phase FSPM machine," *IEEE Trans. Ind. Electron.*, vol. 68, no. 12, pp. 11719–11730, Dec. 2021.

[5] L. Yan et al., "Suppression of major current harmonics for dual three-phase PMSMs by virtual multi three-phase systems," *IEEE Trans. Ind. Electron.*, vol. 69, no. 6, pp. 5478–5490, Jun. 2022.

[6] Y. Luo and C. Liu, "Elimination of harmonic currents using a reference voltage vector based-model predictive control for a six-phase PMSM motor," *IEEE Trans. Power Electron.*, vol. 34, no. 7, pp. 6960–6972, Jul. 2019.

[7] W. Wang, C. Liu, Z. Song, and Z. Dong, "Harmonic current suppression for dual three-phase PMSM based on deadbeat control and disturbance observer," *IEEE Trans. Ind. Electron.*, vol. 70, no. 4, pp. 3482–3492, Apr. 2023.

[8] X. Sun, X. Lin, D. Guo, G. Lei, and M. Yao, "Improved deadbeat predictive current control with extended state observer for dual three-phase PMSMs," *IEEE Trans. Power Electron.*, vol. 39, no. 6, pp. 6769–6782, Jun. 2024.

[9] Z. Hou and S. Jin, "Data-driven model-free adaptive control for a class of MIMO nonlinear discrete-time systems," *IEEE Trans. Neural Netw.*, vol. 22, no. 12, pp. 2173–2188, Dec. 2011.

[10] Y. F. Zhao and T. A. Lipo, "Space vector PWM control of dual three-phase induction machine using vector space decomposition," *IEEE Trans. Ind. Appl.*, vol. 31, no. 5, pp. 1100–1109, Sep./Oct. 1995.